Novel Electronic Structure Induced by a Highly Strained Oxide Interface with Incommensurate Crystal Fields

H. W. Ou,[1,2] J. F. Zhao,[1,2] Y. Zhang,[1,2] B. P. Xie,[1,2] D. W. Shen,[1,2] Y. Zhu,[1] Z. Q. Yang,[1] J. G. Che,[1] X. G. Luo,[3] X. H. Chen,[3] M. Arita,[4] K. Shimada,[4] H. Namatame,[4] M. Taniguchi,[4] C. M. Cheng,[5] K. D. Tsuei,[5] and D. L. Feng[1,2,*]

[1]*Surface Physics Laboratory (National key laboratory) and Physics Department, Fudan University, Shanghai 200433, P. R. China*
[2]*Advanced Materials Laboratory, Fudan University, Shanghai 200433, P. R. China*
[3]*Hefei National Laboratory for Physical Sciences at Microscale and Department of Physics, University of Science and Technology of China, Hefei, Anhui 230026, P. R. China*
[4]*Hiroshima Synchrotron Radiation Center and Graduate School of Science, Hiroshima University, Hiroshima 739-8526, Japan*
[5]*National Synchrotron Radiation Research Center, and Department of Physics, National Tsing-Hua University, Hsinchu 30077, Taiwan, Republic of China*

(Received 12 April 2008; published 15 January 2009)

The misfit oxide, $Bi_2Ba_{1.3}K_{0.6}Co_{2.1}O_{7.94}$, made of alternating rocksalt-structured [BiO/BaO] layers and hexagonal CoO_2 layers, was studied by angle-resolved photoemission spectroscopy, revealing the electronic structure of a highly strained oxide interface. We found that low-energy states are confined within individual sides of the interface, but scattered by the incommensurate crystal field from the other side. Furthermore, the high strain on the rocksalt layer induces large charge transfer to the CoO_2 layer, and a novel effect, the interfacial enhancement of electron-phonon interactions, is discovered.

DOI: 10.1103/PhysRevLett.102.026806 PACS numbers: 73.20.−r, 71.27.+a, 79.60.−i

Oxide interfaces have attracted much attention for the emergence of novel phenomena [1–6]. For example, high conductivity [1] and even superconductivity [2] were discovered at the interface between two insulators, $LaAlO_3$ and $SrTiO_3$; and gigantic thermoelectric power at the $SrTiO_3/SrTi_{0.8}Nb_{0.2}O_3$ interface was discovered five times higher than the bulk material [7]. Clearly, it provides opportunities for promising applications. A thorough understanding of the microscopic processes at the oxide interface is the first step toward designing functional heterostructures. Particularly, it is crucial to find out the electronic behavior at oxide interfaces, e.g., how the electron bands react to two competing, and sometimes incommensurate periodic potentials [8] on both sides of the interface and how they react to strain, and peculiar phonon structures at the interface [5,9]. The answers to these questions would lead to the understanding of the charge transfer process, the insulator-metal transitions, and anomalous transport behavior of the interfaces [3,4,10].

Angle-resolved photoemission spectroscopy (ARPES) is a powerful technique for studying electronic structure of solids and thin films. Pioneering angle-integrated photoemission experiments have been conducted on pulsed-laser deposited oxide interfaces [11–14]. However, because of the short mean free path of photoelectrons, photoemission signals from the interface are very weak, which forbids high resolution and momentum resolved measurements. The recent synthesized misfit oxide single crystals provide an alternative solution [15,16]. Since each unit cell of a misfit oxide is usually composed of two kinds of oxide layers with distinct symmetries, it resembles a very clean artificial heterostructure and is suitable for photoemission experiments. For example, each formula unit of misfit cobaltites, which are known for their anomalously large thermoelectric power, consists of several rocksalt-type MO layers (M = Ca, Sr, Ba, Bi) and one CdI_2-type hexagonal CoO_2 layer with edge-shared CoO_6 octahedra, e.g., $[BaO]_2[BiO]_2[CoO_2]_\alpha$ as shown in Fig. 1(a). The two sublattices of rocksalt (RS) layers and hexagonal layer possess incommensurate lattice constants along one Bi-O-Bi axis, and a commensurate one along the other, causing large strain and a global mismatch of the two lattices.

In this Letter, we report ARPES measurements of a misfit structured oxide, $Bi_2Ba_{1.3}K_{0.6}Co_{2.1}O_{7.94}$ (BBKCO), which reveals the detailed electronic structure of an oxide interface for the first time. We find that large strain in the rocksalt layer induces a large electron transfer to the less strained CoO_2 layer. At the presence of two incommensurate crystal fields, the low-energy electronic states of each individual layer are confined within itself; but they undergo umklapp scattering by the incommensurate crystal field from the neighboring layer. Furthermore, a novel interfacial enhancement of electron-phonon interactions (likely with interfacial phonons) is discovered. These novel electronic properties depict a detailed microscopic picture of various important processes that could occur at oxide interfaces in general.

$Bi_2Ba_{1.3}K_{0.6}Co_{2.1}O_{7.94}$ possesses the highest thermoelectric power and high conductivity in its class, and thus high figure of merit for thermoelectric applications. The single crystals were prepared by the flux method described in detail elsewhere [17]. Its structure is the same as that in Fig. 1(a), with K^+ and Co^{3+} ions doped into the BaO layer. The two adjacent BiO layers are weakly bound by the van der Waals force, providing a stable BiO natural cleavage plane. This is shown by the rectangular low-energy elec-

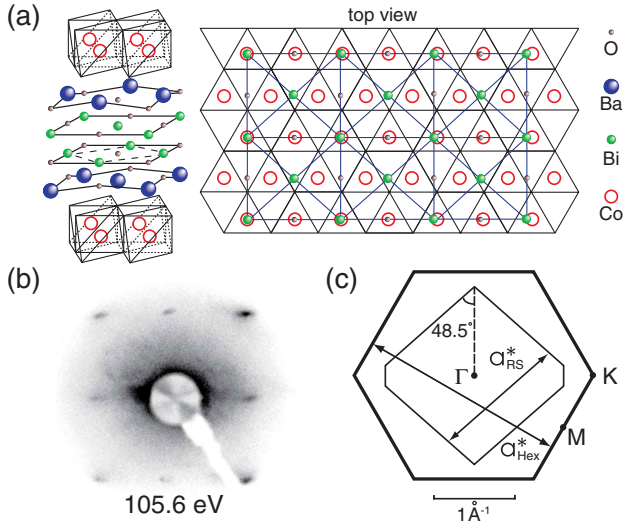

FIG. 1 (color online). (a) A schematic picture of the crystal structure of $Bi_2M_2Co_2O_y$ (M = Ca, Sr, Ba). Oxygen atoms in the CoO_2, and BaO layers are omitted for simplicity in the top view. (b) Low-energy electron diffraction pattern exhibits the fourfold symmetry of the orthorhombic BiO surface of $Bi_2Ba_{1.3}K_{0.6}Co_{2.1}O_{7.94}$. (c) The reduced Brillouin zones for the rocksalt [BiO/BaO] layers (thin lines) and the hexagonal CoO_2 layer (thick lines). The reciprocal lattice constants a^*_{RS} and a^*_{Hex} are illustrated.

tron diffraction (LEED) pattern in Fig. 1(b). The [BiO/BaO] layers are orthorhombic, the lattice constants along the two Bi-O-Bi bond directions are $a_{RS} = 5.031$ Å, $b_{RS} = 5.683$ Å, respectively. a_{RS} matches the distance between the neighboring Co ions along the same direction, while for the perpendicular direction, $b_{RS} = 1.97\ b_{CoO_2}$, which is collinear but aperiodic, causes the global misfit of the lattice. The CoO_2 sublattice preserves the structure of its freestanding form, close to that in Na_xCoO_2 [18]. However, the [BiO/BaO] sublattice is largely distorted compared with the BiO, BaO layers in cuprate superconductors $Bi_2Sr_2CaCu_8O_{8+\delta}$ and $YBa_2Cu_3O_{7-x}$, which are squeezed by 6.4% along the a_{RS} direction, while elongated by about 5.75% along the b_{RS} direction. The Ba^{2+} ions are further displaced from the BaO plane towards the oxygen ions of the CoO_2 layer by 0.4 Å. These huge displacements and the misfit indicate large strain in the rocksalt layer. The reduced Brillouin zones for the individual [BiO/BaO] layers and CoO_2 layer are plotted in Fig. 1(c).

ARPES measurements were performed at beam line 9 of Hiroshima Synchrotron Radiation Center (HiSOR), beam line 5-4 of Stanford Synchrotron Radiation Laboratory (SSRL), and beam line 21 of National Synchrotron Radiation Research Center (NSRRC). The first two beam lines are equipped with a Scienta R4000 analyzer, while the latter is equipped with a SES200 analyzer. Typical energy and angular resolutions are 10 meV and 0.3°, respectively, in the experiments.

Two kinds of states with distinct photon energy dependence are identified for BBKCO. Figures 2(a)–2(f) show the photoemission intensity along the Γ-K direction taken with six different photon energies between 15 and 24 eV. With relatively low-energy photons [Figs. 2(a)–2(c)], photoemission data show only one feature that disperses towards K at higher binding energies. Correspondingly, the map of photoelectron intensity at the Fermi energy (E_F) gives a hexagonal holetype Fermi pocket centered around Γ in Fig. 2(g) (dashed lines). This resembles the Fermi surface (FS) observed in Na_xCoO_2 [19], and its CoO_2-layer origin is demonstrated by the 120° angle between two neighboring sections, and the sixfold symmetry. With higher energy photons, another feature that disperses to the opposite direction becomes dominant [Figs. 2(d)–2(f)]. Correspondingly, in Fig. 2(h), four holetype Fermi pockets show up in the intensity map measured at 21.2 eV, which could be fitted with the four dash-dotted ellipses. These FS's with the symmetry of the rocksalt layer were not observed in previous ARPES works of other misfit Cobaltites [20,21]. Clearly, they should be mostly originated from the [BiO/BaO] layers. The different origins of these bands enable us to unveil various interfacial effects, and explain the observed large photon energy dependence. Since the environment of [BiO/BaO] layer is asymmetric, while CoO_2 layer is symmetric along the c-axis, the distribution of their wave functions along the c-axis are very different. Upon varying photon energy, out-of-plane momentum (k_z) of the final state photoelectron varies. Consequently, the photoemission matrix elements are affected differently for states in different layers [22].

The van der Waals bond between two neighboring BiO layers and the large resistivity anisotropy ($\varrho_c/\varrho_{ab} \sim 10^4$) in BBKCO [17] suggest weak inter-unit-cell coupling. Consistently, the Fermi crossing momenta (k_F's) in Figs. 2(a)–2(f) show negligible dependency on the photon energies, which correspond to different k_z's. For a two dimensional state, one can estimate its occupancy through the FS volume based on the Luttinger theorem [23]. The CoO_2 layers are usually stoichiometric, which would be half filled in undoped case. The measured FS volume indicates that each CoO_2 formula unit has 0.6 extra electrons from the [BiO/BaO] layers. The [BiO/SrO] layers in cuprate superconductors are prototypical charge reservoir, which donate holes to the CuO_2 plane. Normally, one would expect [BiO/BaO] layers to donate holes, especially when its Ba^{2+} ions are replaced with K^+ ions. However, the FS volume of the [BiO/BaO] rocksalt layers indicates that 0.6 *electrons* are missing for each $[BiO/Ba_{0.65}K_{0.3}Co_{0.05}O]$ formula unit, which exactly matches the additional electrons in the CoO_2 layer. This large electron loss out of the [BiO/BaO] layers clearly demonstrates that huge strain would significantly raise the energy of electronic states. Consequently, the electrons flow into the low-energy states of the nearby layer. For BBKCO, this charge transfer would save the total energy significantly, and thus help stabilize the misfit structure [24]. Furthermore, the exact electron and hole concentration match indicates that the systems are very close to its

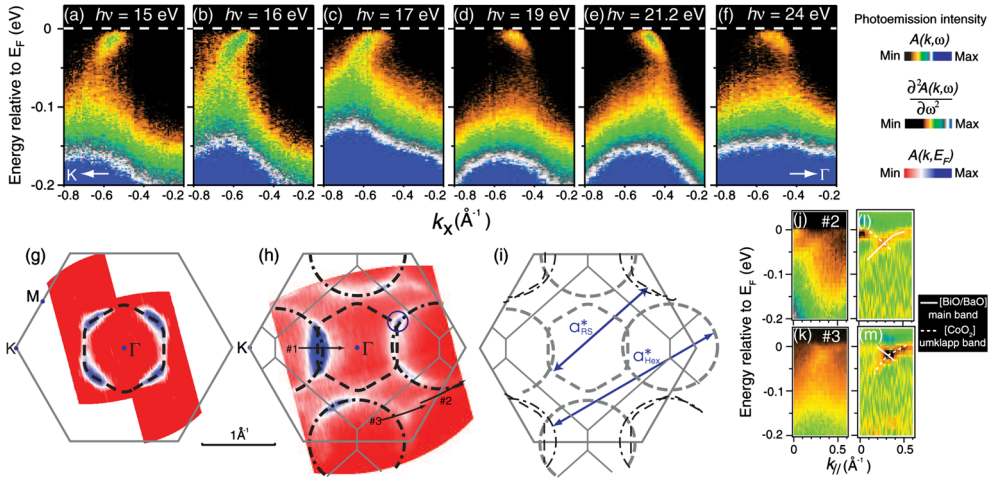

FIG. 2 (color online). ARPES data taken at SSRL for $Bi_2Ba_{1.3}K_{0.6}Co_{2.1}O_{7.94}$ along the cut 1 with (a) 15, (b) 16, (c) 17, (d) 19, (e) 21.2, and (f) 24 eV photon energy. (g), (h) Fermi surfaces (FS) measured at 20 K with 12.5 and 21.2 eV photons from HiSOR, respectively, which are obtained by integration of the spectral weight in a 20 meV window around E_F. The dash-dotted and dashed thick curves are $[CoO_2]$-derived and [BiO/BaO]-derived Fermi pockets, respectively. Their umklapp FS's are indicated by thinner curves in (i). (j), (k) The photoemission intensity along cut 2 and 3 in panel h, respectively, and (l), (m) their second derivative with respect to energy to highlight the dispersion.

stoichiometric condition. Particularly, the quite stoichiometric oxygen concentration in such a highly strained interface is in sharp contrast to the behavior of BiO layer in $Bi_2Sr_2CaCu_8O_{8+\delta}$. This is further confirmed by our wavelength dispersive x-ray analysis (WDX), which can accurately determine the concentration of light elements.

A charge unbalance of $0.6e^-$ for the low-energy states would induce a Madelung potential as large as 24 eV based on an electrostatic calculation [25]. For a realistic Madelung potential difference of 1–2 eV between layers, the *net* charge difference across the interface would be less than 0.025–$0.05e^-$. Therefore, there must be another channel for a "back-flow" of electrons, for example, by forming covalent bonds across the interface in the high lying states [26]. Indeed, the evidence for such covalent bondings is found in the k_z dependence of the valence band dispersion along the Γ-K direction in Fig. 3. The bands below -2 eV disperse differently for the two sampled k_z's, with the largest variation of about 0.5 eV. These bands are mainly of Ba, Bi, and Oxygen character based on our band structure calculations, and the corresponding covalent bonds provide a binding force for the misfit structure. Furthermore, the k_z dispersion shows the long range coherence is preserved despite the varying bond angle and length along the c-axis caused by the misfit.

Strong interlayer couplings were observed for quantum well states at metal-semiconductor interfaces [27]. Remarkably, the low-energy bands in different layers of BBKCO do not show any sign of hybridization, even though there is a large charge transfer in between. For example, in Fig. 2(h), the CoO_2 FS crosses the rocksalt layer FS without any sign of anticrossing. In particular, there is even a slight enhancement of spectral weight at the crossing momentum, as highlighted by the small blue circle. The observed two independent FS sets with distinct symmetries prove that the low-energy electronic states of [BiO/BaO] or CoO_2 layer are spatially confined within itself. This interesting finding is further evidenced by the detailed properties of the quasiparticles. Figures 4(a) and 4(b) show the photoemission images of the quasiparticles in the CoO_2 layer, and the [BiO/BaO] layers, respectively, along the Γ-K direction. As shown in Fig. 4(d), the measured quasiparticle scattering rate is a linear function of the binding energy for CoO_2 state, while it is a quadratic function near E_F for [BiO/BaO] state.

There are several weak FS features besides the main ones in Fig. 2(h). If one would displace the main FS of [BiO/BaO] layers by the reciprocal lattice constant a^*_{Hex} of the CoO_2 layer [illustrated by the double-headed arrows in Fig. 2(i)], the resulting umklapp FS's (thin lines) perfectly fit these weak features in Fig. 2(h). Similarly, the CoO_2 umklapp FS's are observed apart from the main ones by the reciprocal lattice constant a^*_{RS} of the [BiO/BaO] layers.

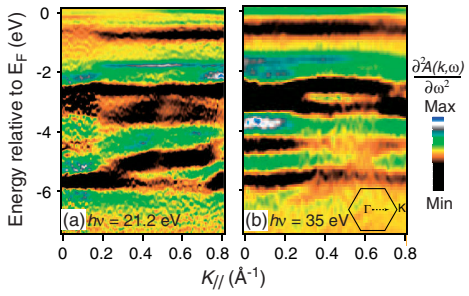

FIG. 3 (color online). Valence band structure determined by the minimum locus of the 2nd derivative of the photoemission intensity along the Γ-K direction taken with (a) 21.2 eV and (b) 35 eV photons, respectively, at NSRRC.

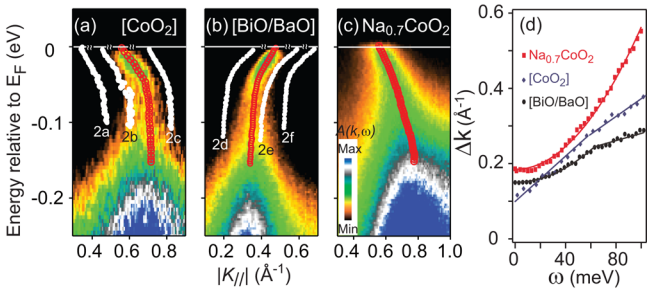

FIG. 4 (color online). Photoemission intensity along Γ-K taken at 20 K in HiSOR, for (a) BBKCO's CoO_2 layer ($h\nu = 15$ eV), (b) BBKCO's [BiO/BaO] layers ($h\nu = 21.2$ eV), and (c) $Na_{0.7}CoO_2$ ($h\nu = 21.2$ eV). The open circles are fitted dispersions. The filled circles are fitted dispersion of data in Figs. 2(a)–2(f) as denoted. Their momenta are shifted for clarity. (d) The width of the momentum distribution curve vs binding energy for data presented in panels (a)–(c), which is an estimate of the quasiparticle scattering rate.

Therefore, this proves that the crystal field from one side of the interface is imposed on the other, and acts as an incommensurate potential that scatters the electrons there. We note that the main [BiO/BaO] band and the umklapp CoO_2 band just cross each other without any sign of hybridization [Figs. 2(j)–2(m)], manifesting the weak coupling between the low-energy electronic states.

More interfacial effects are revealed by comparing the BBKCO data with those of $Na_{0.7}CoO_2$ taken in the same momentum region. While the $Na_{0.7}CoO_2$ dispersion is a smooth curve [Fig. 4(c)] [28], there are strong kinks on the dispersions of the BBKCO bands [Figs. 4(a) and 4(b)]. These kinks are very robust as they show up independent of photon energy, suggesting an intrinsic effect due to interactions with some bosonic modes. Since the doping for CoO_2 layers in BBKCO and $Na_{0.7}CoO_2$ are similar, the magnetic excitations should have similar strength in both cases. Moreover, the spin-polaron effects proposed for the highly electron-doped Na_xCoO_2 ($x \geq 0.7$) would be weak for the BBKCO with 0.6 electron doping [29]. Therefore, the strong kinks here are most likely caused by phonons induced by the highly strained interface. Considering the nonmagnetic nature of the rocksalt layer, and similar kink energy scales, the kink of the rocksalt layer might be caused by the interface phonons as well. This strong coupling is also reflected in the quasiparticle scattering rate [Fig. 4(d)], where a clear turning point around 60 meV appears for both the bands of BBKCO. Furthermore, the scattering rate of $Na_{0.7}CoO_2$ is a simple quadratic function of binding energy, different from the linear behavior of the BBKCO CoO_2 layer. This suggests that the electron-phonon interactions induced by the interface may change the quasiparticle behavior.

To summarize, we have revealed various interfacial electronic properties that have never been observed in oxide interfaces before. The relation between strain and charge transfer across oxide interface is illustrated from a microscopic level. While the interactions between low-energy states on two sides of the interface are weak, interlayer covalent bonding exists between high lying states. The enhancement of electron-phonon coupling and interfacial umklapp scattering are discovered. Our findings provide an electronic structure foundation for understanding oxide interfaces and some important guidelines for designing oxide devices.

We gratefully acknowledge the help from Dr. D. H. Lu and R. H. He during the SSRL experiment, and Professor M. W. Chen for WDX measurements, and the inspiring discussions with Professor Z.-X. Shen, Professor C. Kim, Professor Z. Q. Wang, and Dr. T. Cuk. This work was supported by NSFC, MOST (973 Project No. 2006CB921300), and STCSM of China. SSRL is a user facility of the U.S. DOE, Office of BES.

*dlfeng@fudan.edu.cn

[1] A. Ohtomo and H. Y. Hwang, Nature (London) **427**, 423 (2004).
[2] N. Reyren *et al.*, Science **317**, 1196 (2007).
[3] N. Nakagawa, H. Y. Hwang, and D. A. Muller, Nature Mater. **5**, 204 (2006).
[4] J. Chakhalian *et al.*, Science **318**, 1114 (2007).
[5] A. Tsukazaki *et al.*, Science **315**, 1388 (2007).
[6] S. Altieri, L. H. Tjeng, and G. A. Sawatzky, Phys. Rev. B **61**, 16948 (2000).
[7] H. Ohta *et al.*, Nature Mater. **6**, 129 (2007).
[8] J. Voit *et al.*, Science **290**, 501 (2000).
[9] J.-P. Locquet *et al.*, Nature (London) **394**, 453 (1998).
[10] S. Okamoto and A. J. Millis, Nature (London) **428**, 630 (2004).
[11] H. Kumigashira *et al.*, Appl. Phys. Lett. **84**, 5353 (2004).
[12] M. Takizawa *et al.*, Phys. Rev. Lett. **97**, 057601 (2006).
[13] K. Maekawa *et al.*, Phys. Rev. B **76**, 115121 (2007).
[14] H. Wadati *et al.*, Phys. Rev. B **77**, 045122 (2008).
[15] A. C. Masset *et al.*, Phys. Rev. B **62**, 166 (2000).
[16] H. Leligny *et al.*, C. R. Acad. Sci. Paris II **2**, 409 (1999).
[17] X. G. Luo *et al.*, J. Phys. Condens. Matter **20**, 215221 (2008).
[18] I. Terasaki, Y. Sasago, and K. Uchinokura, Phys. Rev. B **56**, R12685 (1997).
[19] H. B. Yang *et al.*, Phys. Rev. Lett. **95**, 146401 (2005).
[20] Z. Yusof *et al.*, Phys. Rev. B **76**, 165115 (2007).
[21] V. Brouet *et al.*, Phys. Rev. B **76**, 100403(R) (2007).
[22] D. L. Feng *et al.*, Phys. Rev. B **65**, 220501(R) (2002).
[23] For band mapping of more three-dimensional systems, see V. N. Strocov *et al.*, Phys. Rev. B **74**, 195125 (2006); E. E. Krasovskii *et al.*, Phys. Rev. B **75**, 045432 (2007).
[24] The saved energy $v_F^0 \times \Delta k$, where v_F^0 is the bare band velocity of the rocksalt layer ($\sim$1 eV Å), and $\Delta k \approx 0.35$ Å^{-1} is the Fermi pocket radius change due to the charge transfer.
[25] W. H. Xie *et al.*, Phys. Rev. Lett. **98**, 047001 (2007).
[26] Z.-Y. Lu *et al.*, Phys. Rev. B **58**, 13698 (1998).
[27] S.-J. Tang *et al.*, Phys. Rev. Lett. **96**, 216803 (2006).
[28] J. Geck *et al.*, Phys. Rev. Lett. **99**, 046403 (2007).
[29] M. Daghofer *et al.*, Phys. Rev. Lett. **96**, 216404 (2006).